Biochemical and Biophysical Research Communications 417 (2012) 268–273

Contents lists available at SciVerse ScienceDirect

Biochemical and Biophysical Research Communications

journal homepage: www.elsevier.com/locate/ybbrc

A mechanism of action for small heat shock proteins

Eamonn F. Healy [a,*], Peter J. King [b]

[a] Department of Chemistry, St. Edward's University, Austin, TX 78704, USA
[b] Department of Biological Sciences, St. Edward's University, Austin, TX 78704, USA

ARTICLE INFO

Article history:
Received 14 November 2011
Available online 1 December 2011

Keywords:
Mtb
Acr
sHSP
α-Crystallin
Molecular dynamics
Dehydron

ABSTRACT

Molecular dynamics simulations of a fitted multimeric structure of *Mycobacterium tuberculosis* α-crystallin (*Mtb* Acr) identify solvent exclusion from the β_4–β_8 hydrophobic groove as a critical factor driving subunit assembly. Dehydration is also implicated as a determinant factor governing the chaperone activity of the dimer upon its dissociation from the oligomer. Two exposed hydrogen bonds, responsible for stabilizing the β_8–β_9 fold are identified as key mechanistic elements in this process. Based on the overproduction of the chemokine CXCL16, observed after macrophage exposure to *Mtb* Acr, the proteases ADAM10 and ADAM17 are mooted as possible targets of this chaperone activity.

1. Introduction

Tuberculosis, resulting from infection by *Mycobacterium tuberculosis* (*Mtb*), is the leading cause of death worldwide due to a bacterial pathogen. The manifestation of the majority of active tuberculosis disease cases results from re-activation of latent *Mtb* infection acquired years, or decades, previously. It is estimated that fully one third of the world's population harbors latent *Mtb* infection [1]. For such individuals quiescent infection has been correlated with the appearance of the tuberculous granuloma [2], where macrophages containing small numbers of dormant bacteria are surrounded by uninfected macrophages. The immunologic mechanisms that cause granuloma formation have not been completely characterized [3]. Considering the highly cellular encapsulation afforded by the tuberculous granuloma, it has been postulated that nutrient and oxygen deprivation are likely environmental cues that could induce the *Mtb* latency [4,5]. The bacterial protein produced in the largest amount during the *Mtb* early-stage hypoxic response is *Mtb* Acr, an α-crystallin (Acr) homolog encoded by the hspX gene [6]. Acr is a 16.3 kDa protein with homology to the human small heat-shock protein (sHSP) protein α-crystallin [7], and like its human analog has been shown to act as a molecular chaperone by protecting against the aggregation of target proteins [8]. The overproduction of Acr under microaerobic conditions, combined with its heat shock activity, suggests a role for Acr in the establishment of the tuberculous granuloma.

Recent protein microarray data from our group revealed 10 supernatant proteins whose concentrations were increased by at least 2-fold following exposure of murine macrophages to Acr-coated polystyrene beads, when compared to levels for cells exposed to control beads [9]. Of these proteins the chemokine CXCL16 demonstrated the largest change, approximately a 3-fold increase. CXCL16 is a CXC-type chemokine that has been shown to be expressed by a variety of cell types, including antigen-presenting cell types such as macrophages [10–12]. This chemokine has also been associated with recruitment of many of the cell types that are also important in granuloma development including T_H1 type $CD4^+$ T cells, T_C1 $CD8^+$ T cells and natural killer T cells. All these cell types express the cognate receptor for CXCL16. CXCL16 is expressed as a transmembrane protein with a large extracellular domain tethered to the membrane by a mucin-like "stalk". Release of CXCL16 results from activation of one of two *A* Disintegrin and Metalloproteinase (ADAM) proteases, namely ADAM10 or ADAM17 which cleave the stalk region to release the bioactive extracellular domain of CXCL16 [13,14]. These studies have suggested that ADAM17 is primarily responsible for induced release of CXCL16 whereas ADAM10 performs constitutive release of CXCL16. This leads to the possibility that Acr-induced release of CXCL16 involves activation of ADAM10 and/or ADAM17.

The dodecameric character of *Mtb* Acr has recently been determined by nanoelectrospray mass spectrometry [15]. The atomic structure of the related α-crystallin domain from *Triricum aestivum* (wheat) was docked into the *Mtb* Acr density map obtained by electron microscopy to generate the structure shown in Fig. 1A. This fitted structure included the conserved IXI/V motif of the C-terminal extension but omitted the remainder of the C-terminal tail.

* Corresponding author. Fax: +1 512 448 8492.
E-mail address: healy@stedwards.edu (E.F. Healy).

0006-291X/$ - see front matter © 2011 Elsevier Inc. All rights reserved.
doi:10.1016/j.bbrc.2011.11.098

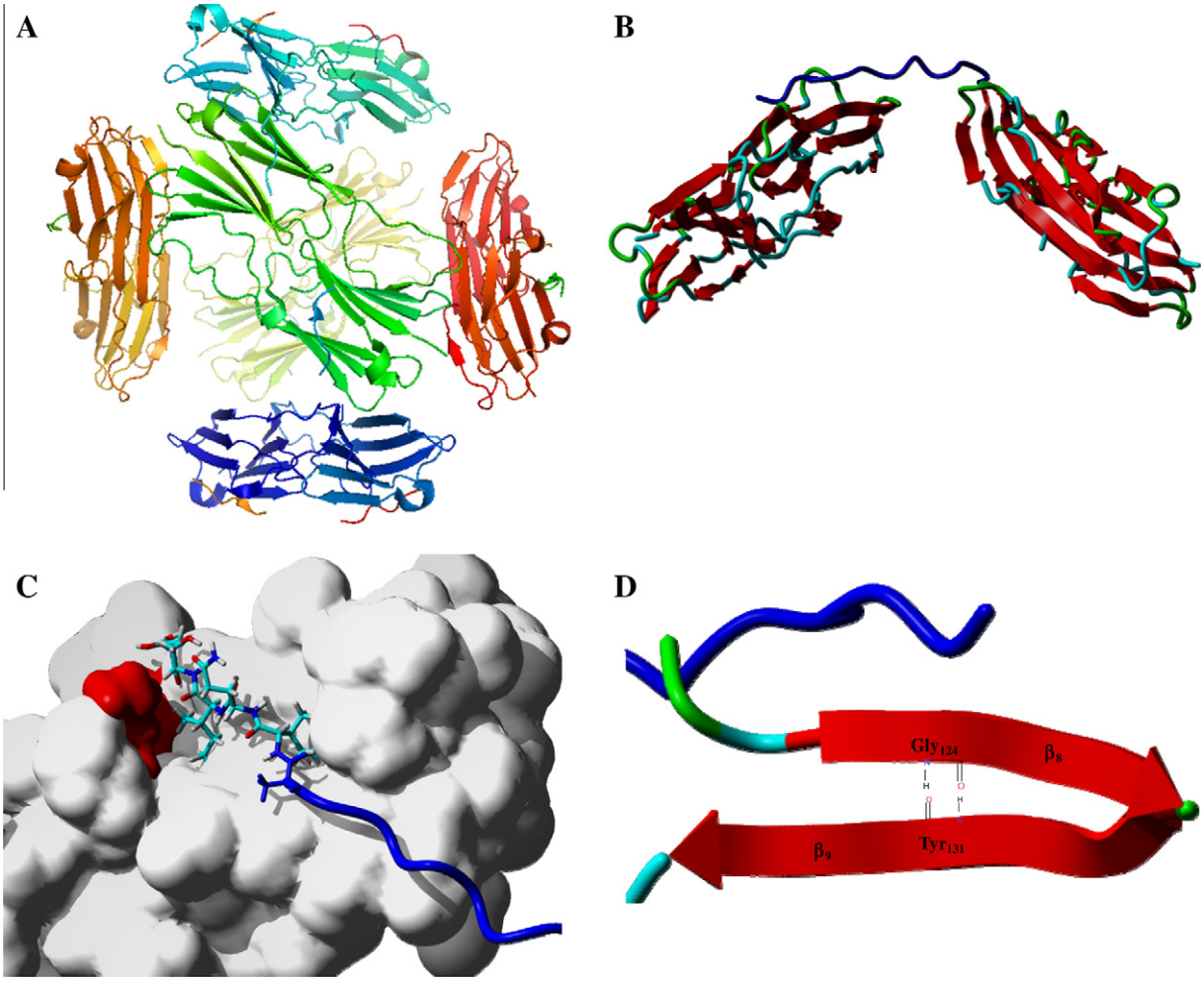

Fig. 1. (A) The dodecamer obtained by fitting the atomic coordinates of the wheat α-crystallin domain to the electron density for *Mtb* Acr (available as pdb code 2BYU). (B) The tetramer from 2BYU after insertion of missing residues in the C-terminal extension. (C) Surface map showing the "patching" of the C-terminal extension into the β_4–β_8 hydrophobic groove, with the IXI/V motif shown in stick and the "plug" residue, Lys_{66}, displayed as red surface. (D) Critical hydrogen bonding interactions linking the β_8 and β_9 strands. (For interpretation of the references to color in this figure legend, the reader is referred to the web version of this article.)

Insertion of the missing residues at positions 138–146, obtained from the wheat structure (available as pdb code 1GME), yields the tetrameric structure shown in Fig. 1B, where the C-terminal loop containing the conserved IXI/V motif of one dimer is shown making intersubunit contact with the adjacent dimer. This structure is consistent with a model of sHSP function in which the larger assembly acts as a reservoir from which the chaperone-active dimer is released to interact with protein targets [16]. The surface image, Fig. 1C, shows the C-terminus extending into the hydrophobic groove formed by the β_4 and β_8 sheets of the neighboring dimer, a motif that has been previously referred to as "patching" [17]. Thermodynamic profiles of sHSP chaperone capacity have identified this dimer–dimer interface as a vital element in conferring the oligomer with a plasticity necessary for the detection of non-native proteins [18]. Critical hydrogen bonding interactions within the Ig fold of the dimer are shown in Fig. 1D.

The chaperone activity of the sHSP dimer of various α-crystallins has been postulated to coincide with the exposure of hydrophobic interface sites after a temperature-regulated subunit exchange or dissociation of the oligomer [19,20]. This provides for exposure of substrate binding sites, that in turn result in the sequestration of the target protein in a high mass complex, thereby preventing formation of an amorphous protein aggregate [16]. Not surprisingly the groove covered by the IXI/V motif has been previously mapped to α-crystallin substrate binding sites [21,22].

Solvent-exposed intramolecular backbone hydrogen bonds, or dehydrons, have been previously identified as vulnerabilities or structural defects in the packing of a wide array of proteins [23,24]. Exposure of such dehydrons to an aqueous environment has previously been shown to weaken protein secondary structures [25,26]. In turn excluding solvent from protein regions containing exposed hydrogen bonds has been implicated as a determinant factor in ligand–protein [27] and protein–protein [28] interactions. Indeed a screening protocol that identifies such structural vulnerabilities, or dehydrons, has been developed [29], and used to guide the rational development of more selective inhibitors [30]. Since dehydron distributions have been shown to correlate with protein subunit assembly [28] as well as playing potentially determinant roles in protein binding, it must be considered highly possible, if not probable, that protection of exposed backbone hydrogen bonds by solvent exclusion plays a role in the chaperone activity of *Mtb* Acr.

2. Methods

The dodecameric structure resulting from the docking of the α-crystallin domain from *T. aestivum* (wheat) into the density map of *Mtb* Acr is available from the RCSB (www.rcsb.org) as Protein Data Bank (pdb) code entry 2BYU. Molecular dynamic (MD) simulations were performed using the tetrameric subunits of 2BYU. This fitted

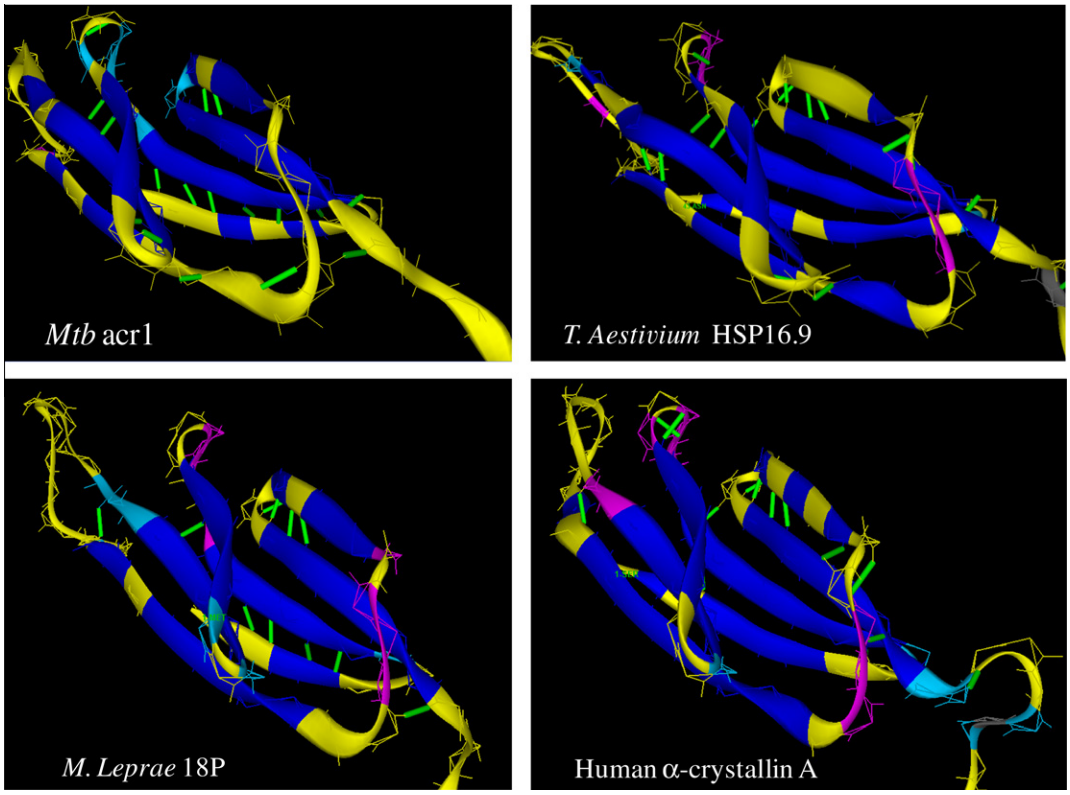

Fig. 2. The α-crystallin domains of four sHSPs with the solvent exposed backbone hydrogen bonds, or dehydrons, identified as green segments connecting the C_α of the linked residues [images generated with YAPView, available from http://sourceforge.net/projects/protlib/files/yapview/].

structure includes the conserved IXI/V motif of the C-terminal extension but lacks the remainder of the C-terminal tail. The missing residues at positions 138–146 were added from the wheat structure (available as pdb code 1GME) after superposition of the backbones of residues 133–138 and 147–151. After adding hydrogens the inserted loop residues and the hydrogen positions were subjected to a short energy minimization using the CHARMm force field [31] as implemented in the Discovery Studio program suite.

Complexes were constructed from the tetramer with and without the IXI/V motif, and solvated with TIP3P explicit water molecules occupying a sphere of radius 25 Å from the C_α carbon of Lys_{66}, and employing an explicit spherical boundary with harmonic restraint. The system was minimized by steepest descent and conjugate gradient. A harmonic restraint was then applied to the dimer containing the C-loop extension, though the IXI/V motif, when present, was left unrestrained and therefore free to move. The complexes were then heated to 300 K, and equilibrated at 300 K for 5 ns. The SHAKE algorithm was employed to keep bonds involving hydrogen atoms at their equilibrium length, allowing the use of a 2 fs time step.

Homology models for the α-crystallin domains of *Mtb* Acr1, *Mycobacterium leprae* 18P and human α-crystallin A were generated from sequence alignments (UniProt P0A5B7, P12809 and P02489, respectively) with the 2BYU homolog, using the MODELER protocol as implemented in the Discovery Studio program suite from Accelrys Inc. The extent of hydrogen bond desolvation is quantified as the number of non-bonded, carbonaceous groups, ρ, contained within a domain centered on the residues linked by the interaction [29]. This desolvation domain is defined as two intersecting spheres of fixed radius centered on the C_α atoms of the linked residues. Dehydrons are then identified as those backbone hydrogen bonds that are underwrapped by non-polar groups, and defined as those interactions with ρ values at or below the average minus one root mean squared deviation. In this work the default values for domain radius, 6.2 Å, and dehydron cutoff, $\rho \leqslant 19$, were used as per reference 29. These dehydrons for the α-crystallin domains of four heat shock proteins are shown as green connectors in Fig. 2.

3. Results and discussion

Given its exposed character the Ig-like β fold structure of Acr provides an almost optimum topology for the presentation of solvent-exposed backbone hydrogen bonds. Dehydron analysis, Fig. 2, identified two solvent-accessible backbone hydrogen bonds conserved across different α-crystallin domains. To test the thesis that this vulnerability is related to patching of the β_4–β_8 hydrophobic groove, 5 nanosecond (ns) MD equilibriations were performed on partially solvated, pre-minimized and pre-heated Acr tetramers, both with and without the IXI/V groove-covering motif. Trajectory analysis of the backbone hydrogen-bonds linking the Gly_{124} residue of the β_8 strand and the Thr_{131} residue of the β_9 strand, Fig. 3, for the final 0.5 ns timeframe clearly confirms these specific inter-strand forces as vulnerable to solvent exposure. From Fig. 3A one can see two diverging trends highlighting the critical role that the IXI/V motif plays in excluding water from the vicinity of the $(Gly_{124})NH$–$O(Thr_{131})$ hydrogen bond. Whereas over the 5 ns equilibriation for the tetramer with the motif inserted into the groove the hydrogen bond actually strengthens over time to a median value of 2.58 Å over the final 500 ps, exposure to water by removing the IXI/V motif reveals a dramatic weakening of this hydrogen bond to a median value over the final 500 ps of 2.83 Å.[1] A similar

[1] A median hydrogen bond distance criteria of ⩽2.7 Å (chosen to accommodate small thermal motions which might result in transient excursion beyond the more generally accepted 2.5 Å limit) and angle criteria 180 ± 60° are taken from reference [32].

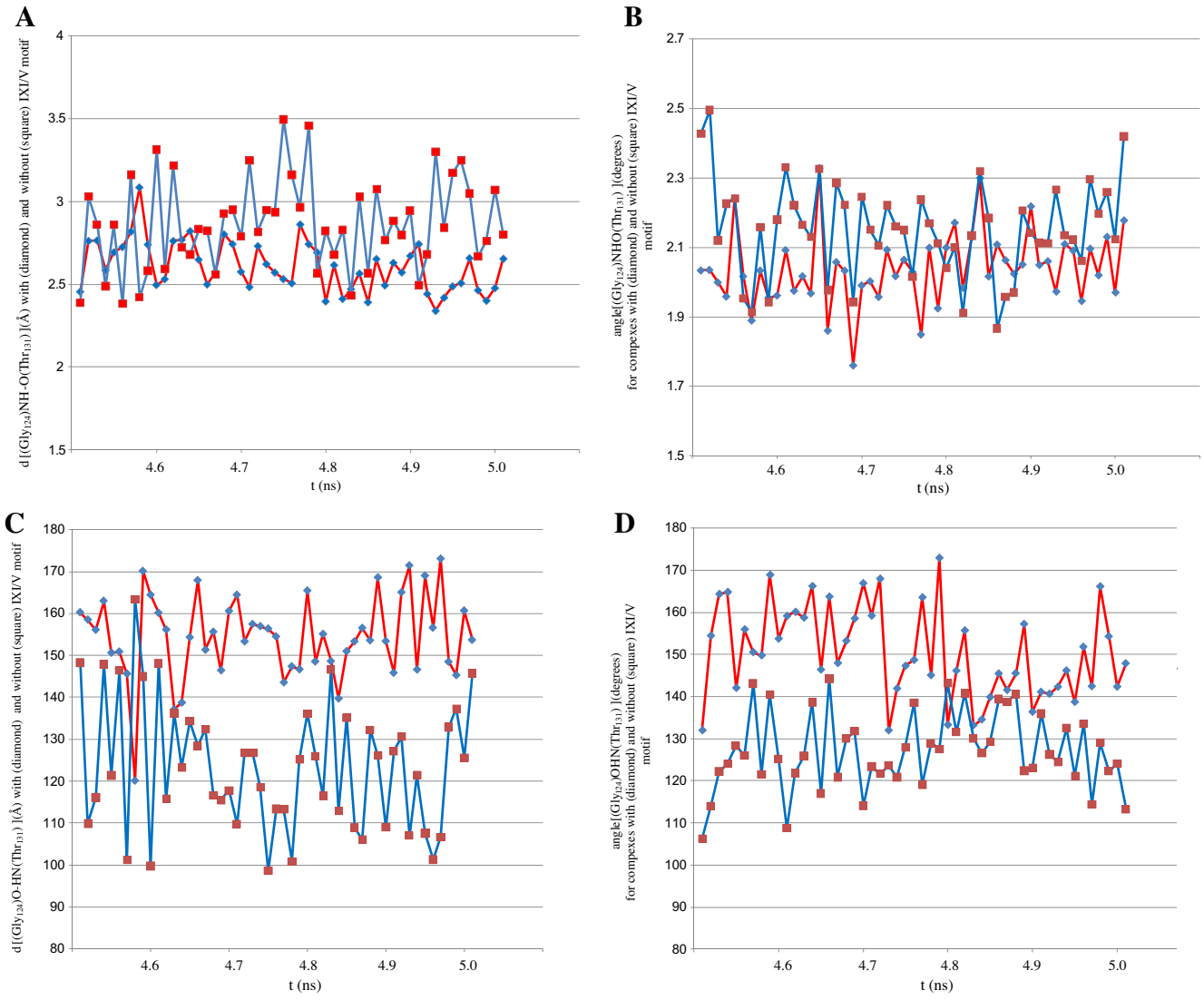

Fig. 3. (A) Trajectory analysis for the (Gly_{124})NH–O(Thr_{131}) hydrogen bond, in Å, for the Acr tetramer with the IXI/V motif (diamond) and without (square). (B) Trajectory analysis for the (Gly_{124})O–HN(Thr_{131}) hydrogen bond, in Å, the Acr tetramer with the IXI/V motif (diamond) and without (square). (C) Trajectory analysis for the (Gly_{124})NHO(Thr_{131}) angle, in degrees, for the Acr tetramer with the IXI/V motif (diamond) and without (square). (D) Trajectory analysis for the (Gly_{124})ONH(Thr_{131}) angle, in degrees, for the Acr tetramer with the IXI/V motif (diamond) and without (square).

trajectory for the (Gly_{124})O–HN(Thr_{131}) hydrogen bond is shown in Fig. 3B and indicates a progressive shortening of the critical donor acceptor distance for both scenarios, with the distance for the solvent exposed tetramer contracting to an average of 2.15 Å over the final 500 ps while the solvent excluded system yields a final average of 2.03 Å. However, trajectory analysis of the putative hydrogen-bond angle (Fig. 3D) identifies that the solvent-exposed interaction regularly fluctuates outside of the 60° tolerance from linearity for the NHO angle [32]. The calculated median value of 125° for the solvent-exposed tetramer over the final 500 ps of equilibriation stands in marked contrast to the median value of 148° calculated for the tetramer with the motif inserted into the groove, where the thermal fluctuations are consistently within tolerance. The angular dependence for the (Gly_{124})NH–O(Thr_{131}) hydrogen bond is also shown in Fig. 3C. Taken together these trajectory analyses indicate that solvent exposure triggers a small but important dislocation of the β_8 strand relative to the β_9 strand, initiated by the migration of solvent molecules towards the underwrapped, and thus exposed, backbone hydrogen bonds (Fig. 4A). This dislocation is sufficient in scope to disrupt key β_8–β_9 inter-strand stabilizing forces. Homology modeling identifies that the Gly_{124}–Thr_{131} inter-strand hydrogen bonding pair is conserved as a Thr_{116}–Thr_{123} interaction in *Mtb* Acr (circled in Fig. 4B).

The ability of sHSPs to interact with a wide range of proteins suggests a rather promiscuous mechanism of action [33]. While some substrate specificity has been associated with hydrophobic loci in the N-terminal arm of certain sHSPs [31], less is known about substrate discrimination for binding sites within the Acr domain [34]. Structural analysis of the alignments of the α-crystallin domains of five sHSPs (human αA and αB crystallin, *Methanococcus jannaschii* HSP16.5, *Mtb* Acr and wheat HSP16.9), Fig. 4B, identifies two residues within the β_4–β_8 hydrophobic groove that, by serving as a topological "plug" for the IXI/V patching motif, could confer some degree of selectivity on the specific sHSP in question. While it has been previously noted that the general architecture of sHSPs favors conservation of the hydrophobic residues proline and leucine at these positions (contained within the L_{34} loop connecting the β_3 and β_4 strands, and the β_8 strand, respectively) [35], the structures for the alignments of wheat HSP16.9 and *Mtb* Acr in Fig. 4B indicate that, even when the hydrophobic character of the residue is not conserved, the orientation of the side-chains of the polar residues, Lys_{66} in wheat HSP16.9 and Tyr_{117} in *Mtb* Acr, is

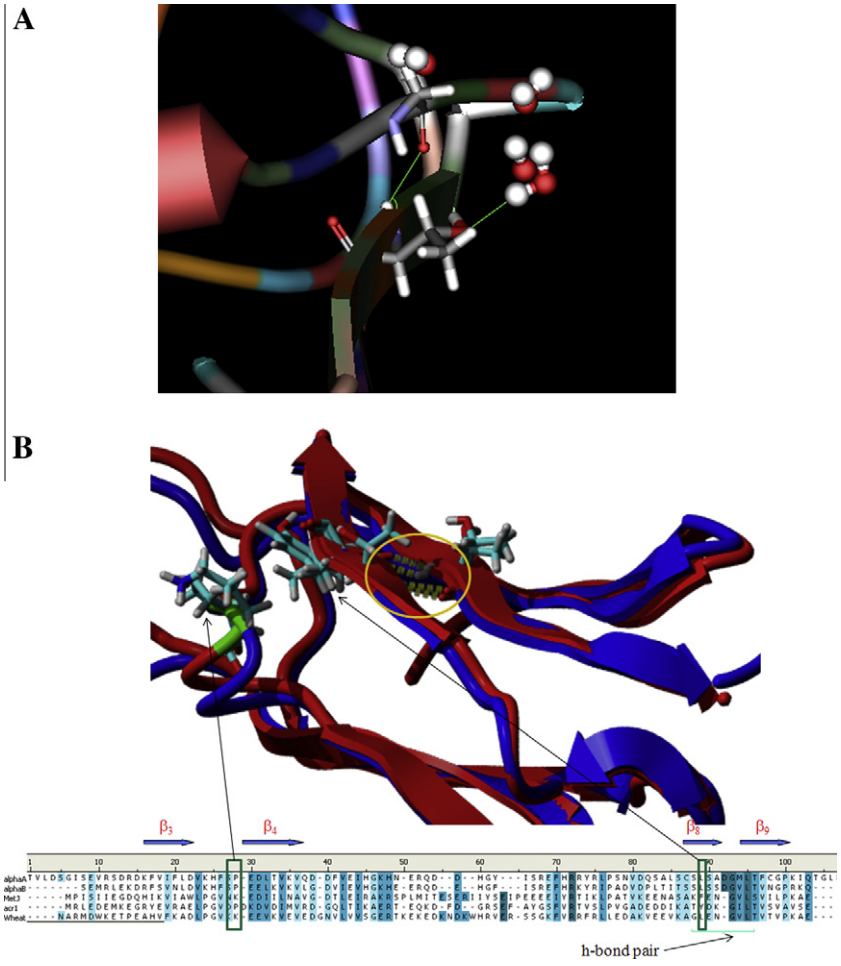

Fig. 4. (A) The β_8–β_9 fold of the 2BYU solvated tetramer without the patching IXI motif, after equilibriation for 5 ns at 300 K. The weakened (Gly_{124})O–HN(Thr_{131}) hydrogen bond and a hydrogen bond between a water molecule and a Tyr sidechain are shown. No hydrogen bond is observed between the Gly_{124} amide and the Tyr_{131} carbonyl, and the dislocation of the β_8 strand relative to the β_9 strand is clearly visible. (B) Sequence alignments for the α-crystallin domains of human αA and αB-crystallin, *Methanococcus jannaschii* HSP16.5, *Mtb* Acr and wheat HSP16.9; homology modeling of the α-crystallin domain of *Mtb* using 2BYU as a template, highlighting residues Lys_{66} and Leu_{125} (wheat), and Pro_{62} and Tyr_{117} (*Mtb*) in stick; the conserved hydrogen bonding pairs for Gly_{124}–Thr_{131} (wheat) and Thr_{116}–Thr_{123} (*Mtb*) are circled.

such that only the non-polar segments of the side-chains are directed towards the interior of the β_4–β_8 groove, thus maintaining the groove's hydrophobic character.

Trajectory analysis of the MD simulations, in conjunction with a structural analysis of the alignment sequences, combine to provide a mechanistic picture of how the release of the chaperone-active dimer of *Mtb* Acr, thus exposing a hydrophobic groove, induces the attachment of a target peptide loop; namely to exclude water and maintain the integrity of the sHSP Ig β-fold. As noted previously the Acr-induced release of CXCL16 implicates two ADAM proteases as possible targets of this Acr heat shock activity. Both of these proteases, ADAM10 and ADAM17, also called TACE, or (tumor necrosis factor α)-converting enzyme, are expressed as zymogens, with large, approximately 200 residue, prodomains maintaining the enzymes in an inactive state. Studies have indicated that the procatalytic domain complex of TACE is inactive due to intramolecular inhibition of the catalytic site by the prodomain [36]. The catalytic site in such a complex is said to be in a *closed* state. However conformational displacement of the TACE prodomain during cellular routing serves to *open* the conformation to yield an enzyme that, while still inactive, now has sites exposed to intracellular proteinases. Proteolytic degradation results in the cleavage of the prodomain to yield a truncate that constitutes the active form of these enzymes. The observed protein microarray data suggests the possibility that *Mtb* Acr has the capacity to facilitate such an activation, which in turn leads to the observed 3-fold increase in CXCL16 release. Taken together with the microarray data the structural model studies above indicate that release of the chaperone-active dimer of *Mtb* Acr exposes a hydrophobic groove, inducing the attachment of a target peptide loop so as to exclude water and maintain the integrity of the sHSP Ig β-fold. If that target peptide sequence is part of either the ADAM prodomain, or possibly the catalytic domain, it could facilitate the conformational change necessary for production of the active enzyme, thus promoting CXCL16 cleavage.

Acknowledgment

E.F.H. wishes to thank the Welch Foundation (Grant No. BH-0018) for its continuing support of the Chemistry Department at St. Edward's University.

References

[1] C. Dye, S. Scheele, P. Dolin, V. Pathania, M. Raviglione, M. Fabian, Global burden of tuberculosis: estimated incidence, prevalence, and mortality by country, JAMA 282 (1999) 677–686.
[2] A. Dannenberg, Pathogenesis of pulmonary tuberculosis: an interplay of tissue-damaging and macrophage-activating immune responses - dual mechanisms that control bacillary multiplication, in: B.R. Bloom (Ed.), Tuberculosis: Pathogenesis Protection and Control, American Society for Microbiology Press, Washington, DC, 1994, pp. 459–483.

[3] P. Hessian, J. Highton, A. Kean, C. Sun, M. Chin, Cytokine profile of the rheumatoid nodule suggests that it is a Th1 granuloma, Arthritis and Rheumatism 48 (2003) 334–338.
[4] L. Via, P. Lin, S. Ray, J. Carrillo, S. Allen, S. Eum, K. Taylor, E. Klein, U. Manjunatha, J. Gonzales, E. Lee, S. Park, J. Raleigh, S. Cho, D. McMurray, J. Flynn, C. Barry, Tuberculous granulomas are hypoxic in guinea pigs, rabbits, and nonhuman primates, Infection and Immunity 76 (2008) 2333–2340.
[5] Y. Hu, A. Coates, Increased levels of sigJ mRNA in late stationary phase cultures of *Mycobacterium tuberculosis* detected by DNA array hybridisation, FEMS Microbiology Letters 202 (2001) 59–65.
[6] D. Sherman, M. Voskuil, D. Schnappinger, R. Liao, M. Harrell, G. Schoolnik, Regulation of the *Mycobacterium tuberculosis* hypoxic response gene encoding alpha-crystallin, Proceedings of the National Academy of Sciences of the United States of America 98 (2001) 7534–7539.
[7] A. Verbon, R. Hartskeerl, A. Schuitema, A. Kolk, D. Young, R. Lathigra, The 14,000-molecular-weight antigen of *Mycobacterium tuberculosis* is related to the alpha-crystallin family of low-molecular-weight heat shock proteins, Journal of Bacteriology 174 (1992) 1352–1359.
[8] Z. Chang, T. Primm, J. Jakana, I. Lee, I. Serysheva, W. Chiu, H. Gilbert, F. Quiocho, *Mycobacterium tuberculosis* 16-kDa antigen (hsp16.3) functions as an oligomeric structure in vitro to suppress thermal aggregation, Journal of Biological Chemistry 271 (1996) 7218–7223.
[9] E.F. Healy, S. Terryah, L. Goering, P.J. King, manuscript in preparation.
[10] M. Matloubian, A. David, S. Engel, J. Ryan, J. Cyster, A transmembrane cxc chemokine is a ligand for HIV-coreceptor bonzo, Nature Immunology 1 (2000) 298–304.
[11] A. Wilbanks, S. Zondlo, K. Murphy, S. Mak, D. Soler, P. Langdon, D. Andrew, L. Wu, M. Briskin, Expression cloning of the STRL33/BONZO/TYMSTR ligand reveals elements of CC, CXC, and CX3C chemokines, Journal of Immunology 166 (2001) 5145–5154.
[12] C.H. Kim, E.J. Kunkel, J. Boisvert, B. Johnston, J.J. Campbell, M.C. Genovese, H.B. Greenberg, E.C. Butcher, Bonzo/CXCR6 expression defines type 1-polarized t-cell subsets with extralymphoid tissue homing potential, Journal of Clinical Investigation 107 (2001) 595–601.
[13] P. Gough, K. Garton, P. Wille, M. Rychlewski, P. Dempsey, E. Raines, A disintegrin and metalloproteinase 10-mediated cleavage and shedding regulates the cell surface expression of CXC chemokine ligand 16, Journal of Immunology 172 (2004) 3678–3685.
[14] A. Ludwig, C. Hundhausen, M.H. Lambert, N. Broadway, R.C. Andrews, D.M. Bickett, M.A. Leesnitzer, J.D. Becherer, Metalloproteinase inhibitors for the disintegrin-like metalloproteinases ADAM10 and ADAM17 that differentially block constitutive and phorbol ester-inducible shedding of cell surface molecules, Combinational Chemistry and High Throughput Screen 8 (2005) 161–171.
[15] C. Kennaway, J. Benesch, U. Gohlke, L. Wang, C. Robinson, E. Orlova, H. Saibi, N. Keep, Dodecameric Structure of the small heat shock protein Acr1 from *Mycobacterium tuberculosis*, Journal of Biological Chemistry 280 (2005) 33419–33425.
[16] H. Ecroyd, J.A. Carver, Crystallin proteins and amyloid fibrils, Cellular and Molecular Life Sciences 66 (2009) 62–81.
[17] R. Stamler, G. Kappé, W. Boelens, C. Slingsby, Wrapping the alpha-crystallin domain fold in a chaperone assembly, Journal of Molecular Biology 353 (2005) 68–79.
[18] H.S. McHaourab, J.A. Godar, P.L. Stewart, Structure and mechanism of protein stability sensors: chaperone activity of small heat shock proteins, Biochemistry 48 (2009) 3828–3837.
[19] L. Gu, A. Abulimiti, W. Li, Z. Chang, Journal of Molecular Biology 319 (2002) 517–526.
[20] D.P. Claxton, P. Zou, H.S. Mchaourab, Structure and orientation of T4 lysozyme bound to the small heat shock protein alpha-crystallin, Journal of Molecular Biology 375 (2008) 1026–1039.
[21] E. Basha, K.L. Friedrich, E. Vierling, The N-terminal arm of small heat shock proteins is important for both chaperone activity and substrate specificity, Journal of Biological Chemistry 281 (2006) 39943–39952.
[22] R.L. van Montfort, E. Basha, K.L. Friedrich, C. Slingsby, E. Vierling, Crystal structure and assembly of a eukaryotic small heat shock protein, Nature Structural Biology 8 (2001) 1025–1030.
[23] A. Fernández, R.S. Berry, Extent of hydrogen-bond protection in folded proteins: a constraint on packing architectures, Biophysical Journal 83 (2002) 2474–2481.
[24] A. Fernández, H. Scheraga, Insufficiently dehydrated hydrogen bonds as determinants of protein interactions, Proceedings of the National Academy of Sciences of the United States of America 100 (2003) 113–118.
[25] E.F. Healy, S. Johnson, C. Hauser, P. King, Tyrosine kinase inhibition: ligand binding and conformational change in c-Kit and c-Abl, FEBS Letters 583 (2009) 2899–2906.
[26] E.F. Healy, The effect of desolvation on nucleophilic halogenase activity, Computational and Theoretical Chemistry 964 (2011) 91–93.
[27] E.F. Healy, P. Romano, M. Mejia, G. Lindfors III, Acetylenic Inhibitors of ADAM10 and ADAM17: in silico analysis of potency and selectivity, Journal of Molecular Graphics and Modellling 29 (2010) 436–442.
[28] A. Fernández, S. Ridgway, Dehydron: a structure-encoded signal for protein interactions, Biophysical Journal 85 (2003) 1914–1928.
[29] S. Maddipati, A. Fernández, Feature-similarity protein classifier as a ligand engineering tool, Biomolecular Engineering 23 (2006) 307–315.
[30] A. Fernández, A. Sanguino, Z. Peng, A. Crespo, E. Ozturk, X. Zhang, S. Wang, W. Bornmann, G. Lopez-Berestein, Rational drug redesign to overcome drug resistance in cancer therapy: imatinib moving target, Cancer Research 67 (2007) 4028–4033.
[31] B.R. Brooks, R.E. Bruccoleri, B.D. Olafson, D.J. States, S. Swaminathan, M. Karplus, CHARMM: a program for macromolecular energy, minimization, and dynamics calculations, Journal of Computational Chemistry 4 (1983) 187–217.
[32] R.B. Sessions, N. Gibbs, C.E. Dempsey, Hydrogen bonding in helical polypeptides from molecular dynamics simulations and amide hydrogen exchange analysis: alamethicin and melittin in methanol, Biophysical Journal 74 (1998) 138–152.
[33] M. Haslbeck, T. Franzmann, D. Weinfurtner, J. Buchner, Some like it hot: the structure and function of small heat-shock proteins, Nature Structural & Molecular Biology 10 (2005) 842–846.
[34] N. Lentze, F. Narberhaus, Detection of oligomerisation and substrate recognition sites of small heat shock proteins by peptide arrays, Biochemical and Biophysical Research Communications 325 (2004) 401–407.
[35] P. Poulain, J.C. Gelly, D. Flatters, Detection and architecture of small heat shock protein monomers, PLoS ONE 5 (2010) e9990.
[36] J.D. Leonard, F. Lin, M.E. Milla, Chaperone-like properties of the prodomain of TNFalpha-converting enzyme (TACE) and the functional role of its cysteine switch, Biochemical Journal 387 (2005) 797–805.